Gamma Rays from the Nuclear Photoeffect in Carbon, Oxygen, and Copper*

A. S. PENFOLD† AND E. L. GARWIN‡
The Enrico Fermi Institute for Nuclear Studies, The University of Chicago, Chicago, Illinois
(Received May 12, 1959)

A NaI crystal was used to study the spectra of gamma rays associated with the giant resonance cross section of the nuclear photoeffect in carbon, oxygen, and copper. The x-ray source was a bremsstrahlung beam whose energy was varied from 19 to 61 Mev. Cross sections for elastic, and mixed elastic and inelastic scattering were measured at 135° to the x-ray beam. The copper cross section has a magnitude which is well predicted by particle photoproduction cross sections coupled with a dipole dispersion theory. The elastic scattering cross section for carbon can be predicted in a similar fashion, but the oxygen cross section cannot. For oxygen, the observed cross section is much larger than the predicted one and this result is explained if narrow, isolated, resonances are an important part of the oxygen photonuclear cross section. The different behavior of carbon and oxygen which is found is consistent with other experiments. The angular dependence of the oxygen elastic scattering cross section near 22 Mev is predominantly dipole with a possible quadrupole admixture. For oxygen, an inelastic scattering cross section was observed which has a threshold at about 26 Mev, a peak at about 30 Mev, and is due to transitions to a state (or states) near 6 Mev. It is interpreted as the result of an overlap of two giant resonance cross sections—one for the ground state and one for the excited state. The consequences of this interpretation to the theory of the nuclear photoeffect is discussed. The yield of gamma rays from O^{15} and N^{15} which follow neutron or proton emission was also studied and several lines were observed, but none above 6.5 Mev. The photonuclear cross sections associated with these lines are estimated to be 45% of the whole photonuclear cross section at 23 Mev.

I. INTRODUCTION

ALL photonuclear cross sections exhibit a giant resonance which, by virtue of its integrated strength, is believed to be electric dipole in character. The resonance energy lies between 14 and 25 Mev for all the elements and it is always well above the thresholds for neutron and proton emission. The probability for decay by gamma-ray emission is therefore very small. The probability for gamma-ray emission back to the ground state (elastic scattering) can be estimated if it is assumed that the giant resonance is dipole in character. In that case, the probability, at the peak of the giant resonance, is about equal to the peak cross section for particle emission divided by $6\pi\lambda^2$. This estimate gives 2% for gold, 0.6% for copper, and 0.2% for carbon.

In spite of the low yields expected for elastic scattering the process deserves study for a number of reasons. First, the multipole character of the giant resonance can be established from the angular dependence of the cross section. Second, dispersion theory[1,2] can be employed to get a connection between the elastic scattering cross section and the total photonuclear cross section. This approach to the determination of photonuclear cross sections has already been employed by Fuller and Hayward[2] who were able to show that elastic scattering cross sections are quite compatible with total cross sections deduced from studies of (γ,n) and (γ,p) reactions—at least for elements of mass 50 or more. For elements lighter than this, their scattering cross sections do not have a giant resonance shape, and considerable photon absorption above 25 Mev is indicated.

The connection which dispersion theory gives between an elastic scattering cross section and the corresponding total cross section is nonlinear. This makes it possible to determine whether or not narrow, isolated, resonances play a significant role in the photonuclear cross sections for the light elements at giant resonance energies.

In addition to elastic de-excitation of giant resonance states, inelastic processes will also take place. Very little is known about the inelastic cross sections. In the case of gold, de-excitation by inelastic processes seems to be as probable as elastic de-excitation.[3] Large inelastic yields have been reported for other substances as well.[4] A study of inelastic cross sections for the light elements can possibly provide information concerning the basic mechanism of the nuclear photoeffect. For example, consider oxygen. The ground state of O^{16} has zero spin and even parity and the photonuclear cross section exhibits a strong resonance at about 22 Mev, according to measured particle photoproduction cross sections.[5,6] The first excited state of O^{16} also has zero spin and even parity,[7] and it is reasonable to assume that this state also possesses a giant resonance. A strong cross section for inelastic de-excitation of the ground-state giant resonance may occur if the latter strongly overlaps the giant resonance for the excited state. The energy at which this overlap takes place should be "model dependent."

The measurement of any of the quantities which have been discussed must take place in the presence of a very

* Research supported by a joint program of the Office of Naval Research and the U. S. Atomic Energy Commission.
† Now at Litton Industries, Beverly Hills, California.
‡ Now at the University of Illinois.
[1] Gell-Mann, Goldberger, and Thirring, Phys. Rev. **95**, 1612 (1954).
[2] E. G. Fuller and E. Hayward, Phys. Rev. **101**, 692 (1956).
[3] L. Meyer-Schützmeister and V. L. Telegdi, Phys. Rev. **104**, 185 (1956).
[4] M. B. Stearns, Phys. Rev. **87**, 706 (1952).
[5] R. Montalbetti and L. Katz, Can J. Phys. **31**, 798 (1953); Montalbetti, Katz, and Goldemberg, Phys. Rev. **91**, 659 (1953); R. Sagane, Phys. Rev. **84**, 587 (1951).
[6] Cohen, Mann, Patton, Reibel, Stephens, and Winhold, Phys. Rev. **104**, 108 (1956); S. A. E. Johansson and B. Forkman, Arkiv Fysik **12**, 359 (1957); D. L. Livesey, Can J. Phys. **34**, 1022 (1956).
[7] F. Ajzenberg and T. Lauritsen, Revs. Modern Phys. **27**, 77 (1955).

strong background arising from "residual" gamma rays —that is, gamma rays coming from the de-excitation of the residual nuclei which are left after particle emission has taken place from the target nuclei. Even for light elements, such as carbon, the yield of residual gamma rays can be as high as 50% of the total photonuclear particle yield at giant resonance energies.[8] In the case of the light elements, where the levels in the residual nuclei are well spaced, these residual gamma rays provide a method for studying the nuclear photoeffect alternative to the study of emitted particles.

The present paper gives experimental data on all the processes which have been discussed for the case of oxygen (99.8% O^{16}). In addition, sufficient data on carbon and copper have been obtained to provide some comparisons among the three substances. The measurements were made with the 100-Mev betatron at the University of Chicago.

II. THE DIPOLE DISPERSION RELATION

The dispersion relation which applies to the dipole photoeffect[2] can be written in the following form:

$$6\pi\lambda\!\!\!^{-2}\sigma_s(E)=[\sigma_a(E)]^2+\left[\frac{2E}{\pi}P\int\frac{\sigma_a(k)}{E^2-k^2}dk+(6\pi\lambda\!\!\!^{-2}\sigma_T)^{\frac{1}{2}}\right]^2, \quad (1)$$

where $\lambda\!\!\!^{-}$ is the wavelength corresponding to energy E, $\sigma_s(E)$ is the elastic scattering cross section, $\sigma_a(E)$ is the total photonuclear cross section, and σ_T is the Thomson scattering cross section for the nucleus (charge Z, mass A). To apply the equation one must assume that *only* dipole transitions are important. The total cross section, σ_a, can be taken equal to the sum of the photoparticle cross sections with little error. The symbol P means to take the principle value of the integral.

If σ_a goes to zero for energies above the giant resonance then Eq. (1) predicts that the elastic scattering cross section will approach a constant value given by

$$\sigma_s(\text{large } E)=\sigma_T\left[\frac{A}{Z}+0.8x\frac{N}{Z}\right]^2, \quad (2)$$

where x is the fraction of exchange forces which appears in the dipole sum rule[9], Equation (2) assumes that the giant resonance exhausts the dipole sum rule. If x is set equal to zero then Eq. (2) becomes the classical expression for the scattering from a body of charge Z and mass Z (coherent scattering by Z free protons).

Equation (1) can be used to make predictions for the elastic scattering cross section. However, the experimental measurements of σ_a are actually average values, $\langle\sigma_a\rangle$, where the average is taken over the resolution function appropriate to the method of cross-section analysis. When $\langle\sigma_a\rangle$ is obtained from a bremsstrahlung yield curve this resolution function is typically 0.5 Mev or more in width.[10] As long as σ_a is smooth and does not vary too rapidly then $\langle\sigma_a\rangle$ will be a good approximation to it.

For the light elements, detailed studies of bremsstrahlung yield curves for the (γ,n) reactions have revealed the presence of fine structure[11] which indicates that the giant resonance may be subdivided into many narrow resonances. In that case $\langle\sigma_a\rangle$ cannot be inserted into Eq. (1) in place of σ_a.

For the special case where σ_a consists of a series of nonoverlapping resonances Eq. (1) can be transformed into a more useful form. In order to get rid of local interference effects in the scattering cross section we define an averaged scattering cross section, $\bar{\sigma}_s(E)$, where this average is taken over an energy interval containing several of the narrow resonances. Then, to a good approximation, one gets

$$6\pi\lambda\!\!\!^{-2}\bar{\sigma}_s(E)=\bar{\sigma}_a{}^p\langle\sigma_a(E)\rangle+\left[\frac{2E}{\pi}P\int\frac{\langle\sigma_a(E)\rangle}{E^2-k^2}dk+(6\pi\lambda\!\!\!^{-2}\sigma_T)^{\frac{1}{2}}\right]^2. \quad (3)$$

In Eq. (3) the peak height of the levels, averaged over several adjacent levels, is denoted by $\bar{\sigma}_a{}^p(E)$. In order to compare the predictions from Eq. (3) with experiment one must take a further average, $\langle\bar{\sigma}_s(E)\rangle$, where the bracket denotes an average over the resolution function of the detector which is employed in the scattering experiment.

For the case of narrow resonances plus a continuum, a more complicated expression than Eq. (3) is necessary. Near the peak of a giant resonance the integrals on the right-hand sides of Eqs. (1) and (3) give essentially zero contribution.

III. EXPERIMENTAL DETAILS

A. The Detector

The energy sensitive detector was a 5-inch diameter by 4-inch thick NaI crystal optically coupled to a type 6364 photomultiplier tube. The whole assembly was contained in styrofoam inside a magnetic shield. The detection geometry is shown in Fig. 1. A plastic anticoincidence counter was located ahead of the NaI to guarantee that no charged particles coming from the direction of the scatterer would be counted. The solid angle of the detector was defined by a lead collimator whose exit diameter was about 2.8 inches. Absorbers of Be and Pb were used at the collimator entrance as shown.

The detector assembly was mounted on an arm which could pivot about the scatterer. The latter was

[8] S. Penner and J. E. Leiss, National Bureau of Standards Report No. 6219, (unpublished).
[9] J. S. Levinger and H. A. Bethe, Phys. Rev. **78**, 115 (1950).
[10] A. S. Penfold and J. E. Leiss, Physics Research Laboratory Report, University of Illinois, 1958 (unpublished).
[11] Katz, Haslam, Horsley, Cameron, and Montalbetti, Phys. Rev. **95**, 464 (1954); A. S. Penfold and B. M. Spicer, Phys. Rev. **100**, 1377 (1955); D. Jamnik, Nuclear Instr. **1**, 324 (1957).

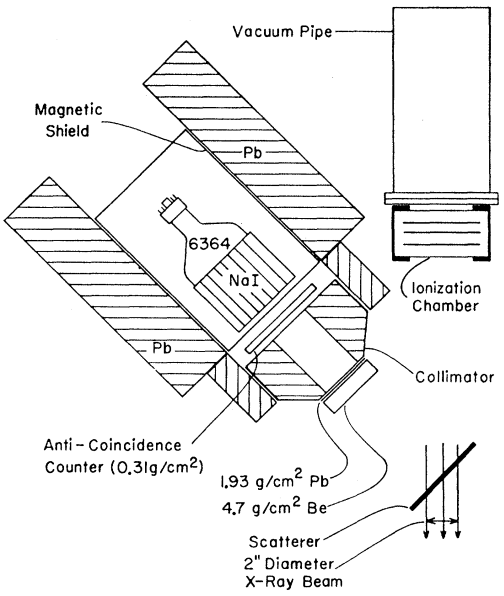

FIG. 1. Sketch of the detector geometry and shielding. Additional shielding which was used is described in the text.

located 5 meters from the x-ray target of the betatron. The diameter of the x-ray beam at the scatterer was set by a Pb collimator located half way between the scatterer and the betatron.

B. The Scatterers

Graphite, water, and copper scatterers were used. In each case the scatterer consisted of a plate of the material mounted at an angle of 45° to the x-ray beam. The water was contained in a $\frac{1}{32}$-inch thick Lucite shell. The thicknesses of the scatterers, measured along the direction of the x-ray beam, were: graphite, 6.0 g/cm²; water, 5.4 g/cm²; copper, 4 g/cm² and 8 g/cm². The scatterers caused an attenuation of the x-ray beam due to pair production and the Compton effect of between 9% and 27% at giant resonance energies.

For measurements made at forward angles the scatterers were rotated 90° from the position shown in Fig. 1.

C. Solid Angle

The solid angle which the detector subtended at the center of the scatterer was not the geometrical one because gamma rays could penetrate parts of the Pb collimator. This effect was calculated for various photon energies. It was found to cause a 10% increase at 15 Mev, for example.

The net effective solid angle at 15 Mev was 0.036 steradian. Corrections to this number due to the finite extent of the scatterer were negligible.

D. Shielding

A great deal of shielding was required in order to keep the background radiation from the betatron suitably small. The primary collimator was 0.20 meter of Pb, located 2.5 meters from the betatron x-ray target. Two secondary collimators were used: one, 0.20 meter of litharge at the betatron donut; the other, 0.25 meter of Pb at 1.8 meters from the betatron. In addition, a shield wall was located after the primary collimator. This wall consisted of 1 meter of Pb shot and 0.25 meter of borax in the immediate vicinity of the x-ray beam, and 2 meters of heavy concrete and 0.25 meter of borax elsewhere.

Electron contamination of the beam was eliminated by a sweep magnet located just after the primary collimator. The beam then entered an evacuated pipe which continued up to the ion chamber monitor as shown in Fig. 1. After leaving the scatterer, the beam traveled 2 meters more and entered the tunnel of a steel "backstop." This device was extremely effective in preventing the residual beam from being reflected from the back wall in the direction of the detector. The borax shield wall reduced the background of photoneutrons which were generated in the Pb of the shield wall. Tests with a neutron long counter were made and it was found that additional borax shielding made very little difference.

The shielding used around the detector assembly is shown in Fig. 1. No Pb shield was employed either above or below the detector. The room in which the measurements were made had a very high ceiling and the beam was 63 inches above the floor. It was found that top or bottom shielding did more harm than good.

A shield consisting of 10 cm of Pb and 25 cm of borax was mounted on an arm which pivoted about the same point as the detector assembly. This shield was positioned diametrically opposite the detector and protected the lightly shielded front face of the detector from room background. It was found very helpful when scattering at angles forward of 90° was being measured.

The Be and Pb shielding used in front of the detector (Fig. 1) was essential in order to reduce pile-up of small pulses in the NaI. The Be functioned as an electron shield, and the Pb functioned as a shield for soft gamma rays.

The anticoincidence shield (Fig. 1) was only useful for angles forward of 90°. By placing this counter in coincidence with the NaI the charged particle flux could be determined. This procedure was used while determining the general shielding requirements.

A previous experiment[2] employed a thick Al filter in the x-ray beam in order to preferentially attenuate low-energy photons. Tests were made to determine the effectiveness of such a filter for this experiment, and it was found to be unnecessary.

E. Monitoring

The transmission type ion chamber shown in Fig. 1 was employed to monitor the x-ray intensity. The charge transferred by the chamber was collected on a

polystyrene condenser whose voltage was read with a vibrating reed electrometer. The transmission chamber was calibrated against a thick Cu ion chamber[12] of known response.[13]

F. Electronics

The data was recorded on a 50-channel pulse-height analyzer of the pulse-to-digital type. The analyzer was capable of handling pulses with a rise time of 50 mμsec and had a voltage sensitivity of 1 volt/channel. The net amplification used between the photomultiplier tube and the analyzer was 1.8.

The pulses at the photomultiplier anode had a full rise time of 0.2 μsec. They were then processed by a pulse shaping circuit and presented to a linear gate[14] of 0.2-μsec duration. The pulses presented to the gate were bipolar and of 0.5 μsec full width. The gate was controlled by a fast trigger branch of the circuits and it opened only for pulses which: occurred during the x-ray period (60 bursts per second); were not accompanied by a count in the anticoincidence counter; were big enough to record above channel 8 on the analyzer.

Tests with a light pulser showed that the light-to-voltage transfer characteristic of the detector was linear over the operating range used. Tests with a sliding pulser showed that the voltage-to-channel transfer characteristic of the system departed from linearity by less than 0.05 channel between the 50th and the 16th channel, and by 1 channel between the 16th and the 6th. All data which were used were recorded from channel 15 and up. The output pulse of the sliding pulser was carefully shaped to be the same as the photomultiplier pulses.

The photomultiplier gain was monitored before and after each irradiation through the use of a Na^{22} source. The electronic gain was monitored at least twice a day by means of a pulser. The electronic gain was constant to 1% over long periods of time.

Pulse pile-up was measured by mixing standard, flat-topped, pulses in with the normal train of pulses from the detector. The linear gate was arranged to open only for these standard pulses. When the x-ray intensity was reduced to zero the standard pulses all recorded in one channel in the analyzer. In the presence of x-rays, the pulses spread into more than one channel due to pile-up of small pulses. Because of the bipolar nature of the pulses presented to the linear gate, the effect of pile-up was always a symmetric broadening. In all cases it was kept below ±1 channel. In order to accomplish this the betatron had to be operated at reduced intensity for measurements made at forward angles.

[12] P. D. Edwards and D. W. Kerst, Rev. Sci. Instr. **24**, 490 (1953).

[13] Leiss, Pruitt, and Schrack, National Bureau of Standards Report No. 6149 (unpublished).

[14] E. L. Garwin and A. S. Penfold, Rev. Sci. Instr. **28**, 116 (1957).

G. X-Ray Beam

The x-ray pulse was adjusted to be flat-topped, and its length varied from 30 to 350 μsec depending on the energy being used. The energy spread due to the pulse length was kept at about ±0.4 Mev for all irradiations. The betatron energy scale was known to ±1.5%.

H. Backgrounds

There were two sources of background which did not involve the scatterer: cosmic rays, and room background. Because of the electronic gating, the former was quite small. Typically it amounted to 3 counts/Mev/hour near 22 Mev. At a detector angle of 135° the room background was small compared to the cosmic-ray background for all detector energies above 12 Mev and for all betatron energies up to 60 Mev. For detector angles forward of 90° the room background was appreciable, and for angles less than 45° it was very large.

Non-nuclear x-ray attenuation processes in the scatterer contribute a gamma-ray yield which constitutes a background to the nuclear processes under study. There are two methods for determining the effect of such processes: one is to study the yield as a function of the thickness of the scatterer; the other is to study the angular distribution as the detector is rotated to forward angles. Non-nuclear processes give yields which are sharply peaked forward for energies of interest here. This type of background was found to be serious for graphite and water scatterers for detector angles less than 60°, at 20-Mev detector energy and 30-Mev betatron energy. For copper it was serious for all angles less than 90°. The copper data was taken for two different thicknesses of scatterer (at 135°) and the results indicated that the data were free of this type of background.

A further source of background arises from photoneutrons generated in the scatterer. These give rise to gamma rays from $(n,n'\gamma)$ and (n,γ) reactions in the Pb shield around the detector and in the detector itself. This type of background can be detected by stopping up the detector collimator with a thick piece of Pb. It was experimentally demonstrated that this type of background had a negligible effect on the data presented here.

IV. DETECTOR ENERGY RESOLUTION

Monochromatic gamma rays incident on the NaI detector give rise to a spread of pulse heights from the photomultiplier. For the size of detector used in this experiment, and for gamma rays of 11 Mev or more, the pulse-height distribution function (resolution function) is single-peaked[15] and has the general shape shown by the curve marked $G(y)$ in Fig. 2. This curve is, in fact, the resolution function which was experimentally

[15] H. W. Koch and J. M. Wyckoff, National Bureau of Standards Report No. 5866 (unpublished).

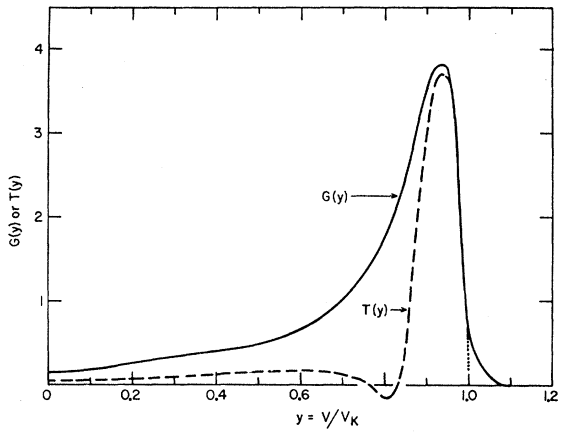

FIG. 2. The detector resolution functions. $G(y)$ is the resolution function which was observed for 15.1-Mev gamma rays, and the same shape was assumed for all energies above 11 Mev. $T(y)$ is the resolution function remaining after cross section analysis (the residual resolution function).

observed for the 15.1-Mev gamma-ray line[16] from C^{12}. The full width of the curve at half maximum is about 18%.

The manner in which the NaI resolution function varies with gamma-ray energy depends on the area of the crystal face which is bathed with the radiation, and also on the individual characteristics of the crystal. The counter assembly shown in Fig. 1 was tested in monoenergetic electron beams of from 15 to 50 Mev, and the percent resolution was found to remain constant. In fact, the resolution function was found to be "universal."

For the analysis of the present experiment the NaI resolution function was assumed to be universal for gamma rays as well, and to have the shape given by $G(y)$ in Fig. 2—the shape which was measured for 15.1-Mev gamma rays. This assumption was tested experimentally with a 44-Mev bremsstrahlung beam. The experimental points shown in Fig. 3 (with some representative statistical errors) were obtained from the pulse-height spectrum observed for a 44-Mev bremsstrahlung beam. The dashed curve gives the shape expected for a detector of infinitely good resolution. The solid curve was generated from the dashed one by folding in the assumed resolution function, $G(y)$. The observed data and the calculated curve are seen to have the same shape to within the experimental uncertainty and so the resolution function $G(y)$ is satisfactory for high energies as well as for low ones. It should be noted, however, that this test is not sensitive to the low-energy tail of $G(y)$.

Let $S(k,V)$ be the probability that a photon of energy k, which interacts in the detector, will give rise to a pulse of height V, per unit range of V. The integral of $S(k,V)$ over all values of V must equal 1. Since $G(y)$ is already normalized to unit area with respect to V/V_k (see Fig. 2), one has

$$S(k,V)=G(V/V_k)/V_k. \tag{4}$$

In Eq. (4) and Fig. 2 the parameter V_k is equal to the value of V at the high-energy cutoff of the resolution function (indicated by the dotted line in Fig. 2). The numerical value of V_k depends on the gain of the detector system, but it is assumed to be linearly related to photon energy, k.

V_k was evaluated before *each* experimental irradiation by swinging the detector into the bremsstrahlung beam and recording the pulse-height distribution of the beam. If the maximum pulse height observed is denoted by V_χ, and the maximum photon energy in the beam by χ, then

$$V_k=kV_\chi/\chi. \tag{5}$$

The determination of V_χ was usually subject to an error of ± 0.5 channel (at about channel 30). This accuracy was only possible when the broadening due to pile-up of small pulses was kept less than ± 0.5 channel.

For purposes of analysis it is convenient to introduce the dimensionless parameter y, which is defined as follows:

$$y=V/V_k=\chi V/kV_\chi. \tag{6}$$

V. ANALYSIS OF DATA

A. General Description

Each experimental irradiation lasted about 100 minutes and yielded a pulse-height spectrum and a monitor reading. The pulse-height spectra were corrected for lost counts and then for cosmic-ray and room background. The lost count correction, which seldom exceeded 10%, was required because the pulse-height

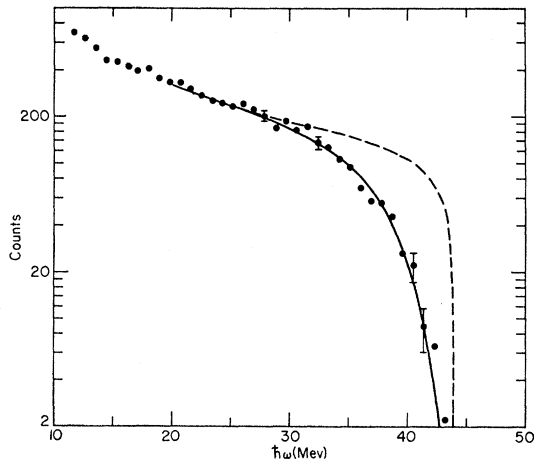

FIG. 3. An experimental test of the resolution function $G(y)$ of Fig. 2. The solid dots give the pulse-height spectrum observed for a 44-Mev bremsstrahlung beam. The dashed curve gives the results expected for a detector of infinitely good resolution, and the solid line gives the results calculated for a detector with resolution $G(y)$. The solid curve was normalized to the experimental measurements at about 22 Mev.

[16] E. L. Garwin, Phys. Rev. **114**, 143 (1959).

analyzer could accept no more than one count per x-ray burst. It was obtained by comparing the number of analyzed counts with the number of times the linear gate presented a pulse to the analyzer for analysis.

The pulse-height spectra were analyzed for differential cross section as if only elastic scattering had occurred. A search for inelastic processes was then made by studying the results as a function of betatron operating energy.

The method of analysis made a partial correction for the resolution function of the NaI detector in that it essentially removed the effects of the low-energy tail of $G(y)$. The remaining resolution function had the form $T(y)$ given in Fig. 2. The effect of the low tail of $T(y)$ was estimated, in retrospect, to have influenced the answers by less than 1% in all cases.

It is interesting to note that the transformation of $G(y)$ into $T(y)$, which the analysis accomplished, resulted in an increase in statistical uncertainty of only 20%.

B. Details of the Analysis

Assuming elastic scattering only, a reaction probability, $W(\theta,k)$, can be defined. It is the probability that a photon of energy k was scattered into the detector and reacted with it

$$W(\theta,k)=\eta\sigma(\theta,k)\Omega(k)\epsilon(k)f(k), \tag{7}$$

where: η is the number of nuclei/cm^2 in the scatterer; $\sigma(\theta,k)$ is the differential cross section for elastic scattering in the direction of the detector; $\Omega(k)$ is the solid angle subtended by the detector at the scatterer (as explained in Sec. III the solid angle was a function of k); $\epsilon(k)$ is the probability that a photon which enters the detector will undergo a reaction there; and $f(k)$ is the probability that a photon will *not* react in either the scatterer or the material situated between the scatterer and the detector.

The pulse-height spectrum resulting from an irradiation at betatron energy χ and detector angle θ is

$$N(\chi,\theta,V)=M(\chi)\int_0^\infty dk\, S(k,V)W(\theta,k)I(\chi,k)/k, \tag{8}$$

where $N(\chi,\theta,V)$ is the number of pulses per unit pulse-height range at pulse height V, $M(\chi)$ is the number of x-ray monitor units recorded, $S(k,V)$ is the detector resolution function, and $I(\chi,k)/k$ is the number of photons of energy k, per unit range of k, which impinged upon the scatterer per unit of monitor response. $I(\chi,k)$ is thus the bremsstrahlung intensity spectrum.

The efficiencies $\epsilon(k)$ and $f(k)$ were calculated from a table of narrow-beam x-ray attenuation coefficients.[17] It turned out that the product $\Omega(k)\epsilon(k)f(k)$ was independent of k. Values for $I(\chi,k)$ were calculated from a table of bremsstrahlung spectra,[10] and from the known monitor response.

Approximate solutions for $W(\theta,k)$ were obtained by a method very similar to that used for the solutions of bremsstrahlung yield curves.[10] The major difference was that, here, it is the NaI resolution function which one desires to remove rather than the bremsstrahlung spectrum.

The solutions were obtained in terms of a linear combination of the measured values of $N(\chi,\theta,V)$. The linear combination was specified by two sets of numbers: B_i and b_i. The solutions are

$$W(\theta,k_V{}^\chi)=\frac{\sum_i B_iN(\chi,\theta,b_iV)}{M(\chi)\int_0^\infty dk\,\dfrac{I(\chi,k)}{k}\sum_i B_iS(k,b_iV)}, \tag{9}$$

where $k_V{}^\chi$ is the centroid of the integrand in the denominator.

Using Eqs. (4) through (6) for the resolution function, Eq. (9) can be rewritten in a form more convenient for computations.

$$W(\theta,k_V{}^\chi)=\frac{V\sum_i B_iN(\chi,\theta,b_iV)}{M(\chi)\int_0^\infty dy\, I(\chi,\chi V/yV_\chi)\sum_i B_iG(b_iy)}. \tag{10}$$

The solutions given by (10) will be satisfactory only if the numbers B_i and b_i can be chosen so that the integrand in the denominator is essentially different from zero only over a small range of y, and if $W(\theta,k)$ is approximately linear over the corresponding range of k.

The form of $G(y)$ (Fig. 2) and the rather poor statistics of the data dictated that only two terms should be used in the linear combination specified by the numbers B_i and b_i. A suitable combination was found by trial and error, and it was

$$\sum_i B_iN(\chi,\theta,b_iV)=N(\chi,\theta,V)-0.564N(\chi,\theta,1.12V), \tag{11}$$

and correspondingly

$$\sum_i B_iG(b_iy)=T(y)=G(y)-0.564G(1.12y). \tag{12}$$

The residual resolution function $T(y)$, which is defined by Eq. (12), is plotted as the dashed curve in Fig. 2. It is analogous to the weighting functions discussed in reference 10.

The numerical computations were greatly simplified by the discovery that the values of $k_V{}^\chi$ [Eq. (9)] and the integral in Eq. (10) could be expressed in a relatively simple way through the use of two empirically determined functions $u(V/V_\chi)$ and $w(V/V_\chi)$. The relations which were found were

$$k_V{}^\chi=\chi u(V/V_\chi), \tag{13}$$

$$\int_0^\infty dy\, I(\chi,\chi V/yV_\chi)T(y) = I(\chi,\chi w[V/V_\chi])\int_{0.8}^1 dy\, T(y). \tag{14}$$

[17] G. R. White, National Bureau of Standards Report No. 1003 (unpublished).

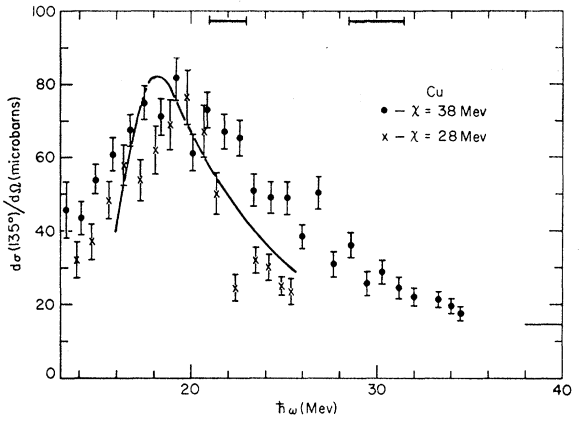

FIG. 4. The scattering cross section for Cu at 135°. The data is for irradiations at bremsstrahlung energies of 28 and 38 Mev. The cross sections are for mixed elastic and inelastic scattering as defined by Eq. (15) in the text. The solid curve is a predicted cross section (see text for details).

Because of the high-energy limit to the bremsstrahlung spectrum at $k=\chi$ the second term in the linear combinations (11) and (12) was dropped for values of V/V_χ greater than 0.8. In no case was the analysis carried to greater values of V/V_χ than 0.95.

C. Inelastic Processes

The method of analysis which has been described is based on the assumption that all gamma-ray yield is due to elastic processes. Inelastic processes can be included by defining a reaction probability analogous to $W(\theta,k)$ which applies to the case where the incident photon has energy k but the detected photon has energy k'. If this probability is $W(\theta,k,k')$, then the solutions which are obtained [Eq. (10)] are actually values for

$$W(\theta,k_{V^\chi})+\frac{k_{V^\chi}}{I(\chi,k_{V^\chi})}\int_0^\infty dk\,\frac{I(\chi,k)}{k}W(\theta,k,k_{V^\chi}). \quad (15)$$

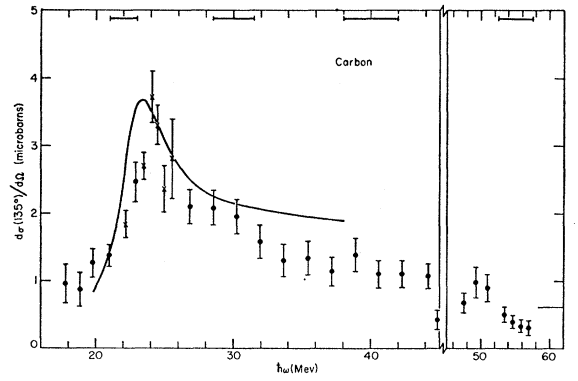

FIG. 5. The scattering cross section for C at 135°. The crosses designate points which can only be due to elastic scattering, while the dots designate points for mixed elastic and inelastic scattering. The mixing is defined by Eq. (15) in the text. The data were obtained from irradiations with bremsstrahlung energies of 27, 28, and 61 Mev. The solid curve is a predicted cross section (see text for details).

The elastic and inelastic processes can then be untangled by studying Eq. (15) as a function of χ. Henceforth, when the term mixed elastic and inelastic scattering is used, it will refer to mixing as defined by Eq. (15).

VI. EXPERIMENTAL RESULTS

The experimental results are shown in Figs. 4 to 9. Differential cross sections measured at 135° to the x-ray beam are given in Figs. 4 to 7 and in each case the heavy horizontal lines along the top of the figures give the full width at half maximum of the residual resolution function [$T(y)$ of Fig. 2]. The light horizontal line near the lower right-hand corner of each figure gives the high-energy limit to the elastic scattering cross section which is obtained from Eq. (2) with no exchange forces and a dipole angular dependence to the cross section. The factor which converts from total cross section to 135° cross section for dipole radiation is $(11.2)^{-1}$.

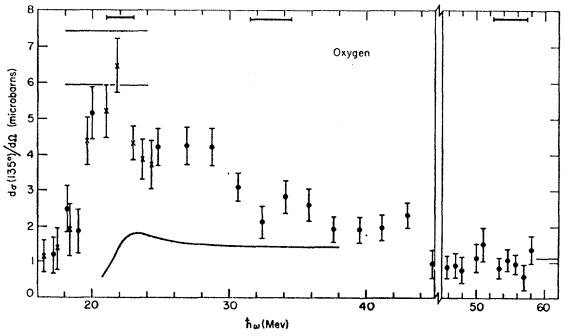

FIG. 6. The scattering corss section for O at 135°. The crosses designate points which can only be due to elastic scattering, while the dots designate points for mixed elastic and inelastic scattering. The mixing is defined by Eq. (15) in the text. The data were obtained from irradiations with bremsstrahlung energies of 22.3, 26.4, and 61 Mev. The solid curve and the light horizontal lines (upper right) are predicted values for the cross section (see text for details).

The errors which are shown are those due to counting statistics only. Additional errors of a systematic nature which may be present are estimated to be about ±15% and are due to uncertainties connected with the height of the low-energy tail on the NaI resolution function; the determination of the detector solid angle; and the absolute monitoring of the intensity of the bremsstrahlung beam.

The solid curves shown on Figs. 4, 5, and 6 give elastic scattering cross sections predicted from the dispersion equation [Eq. (1)] and published photoparticle cross sections. Although no errors are indicated for these predictions, the uncertainties are rather large. Since the published photoparticle cross sections generally are not accompanied by any estimate of error it is not possible to give anything but a very rough estimate of the errors to be associated with the scattering predictions. We estimate the errors to be ±1 Mev on the energy scale, and at least ±20% on the cross-section scale.

A. Copper

The results for Cu are shown in Fig. 4 where the crosses and dots refer to data from irradiations with 28- and 38-Mev bremsstrahlung, respectively. The cross sections are not for elastic scattering, but for mixed scattering as defined by Eq. (15). Since the results do depend on the bremsstrahlung energy, the presence of inelastic scattering is indicated.

The general character of the Cu cross section is that of a single scattering resonance. The peak cross section is about 20 times larger than the Thomson cross section for Cu, and it occurs at an energy roughly coincident with the peak of the gamma-neutron cross section for Cu.

The cross section for a classical dipole oscillator consisting of N neutral masses elastically coupled to Z positively charged masses was calculated. The 28-Mev Cu data can be fitted (in shape) by such a cross section for a resonance energy at 17 Mev, a value in reasonable agreement with experiment.[18] The classical oscillator

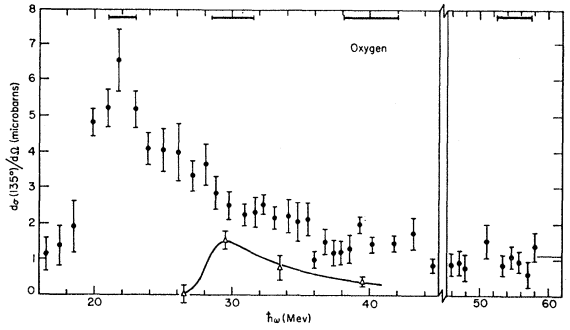

FIG. 7. The elastic scattering cross section for O at 135° (dots) and an inelastic cross section due to transitions to a state near 6 Mev (triangles).

yields too small a peak cross section, but if the calculations are extended to include exchange forces, [Eq. (2) must result in the high-energy limit] a good absolute fit is obtained for 30% exchange.

The solid curve in Fig. 4 is the elastic scattering prediction. The value for the absorption cross section, σ_a, needed for the calculation was obtained by multiplying the measured photoneutron cross section[19] for natural Cu by the published ratio of neutron to charged particle yields,[20] with the deuteron yield omitted. This latter step is required because the (γ,d) cross section is negligible at the peak of the (γ,n) cross section.[20] The prediction given in Fig. 4 is considerably lower than a previously published prediction[2] due to the different, and presumably better, values for σ_a.

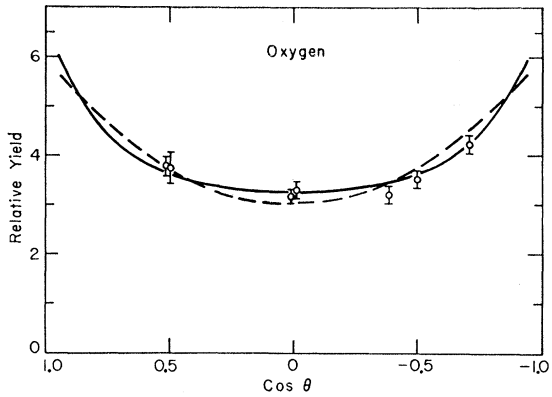

FIG. 8. The angular dependence of the elastically scattered gamma rays from O which lie in the range 19 to 25 Mev. See text for explanation of the dashed and solid lines.

Stearns[4] has measured the 116° scattering cross section for Cu for 17.6-Mev gamma rays. When translated to 135° (assuming a dipole dependence) her value is 55±25 microbarn/sterad, in agreement with the data of Fig. 4. The Cu scattering measurements of Fuller and Hayward[2] are about 1.6 times larger than the results obtained here.

Inelastic scattering of high-energy gamma rays is definitely indicated by the data of Fig. 4, and there is no way of estimating how much inelastic contribution is still contained in the 28-Mev curve. On the basis of energetics it is possible to have inelastic scattering yield in the 38-Mev data due to gamma rays from residual nuclei resulting from neutron or proton emission. Such gamma rays can have energies of 28 Mev or less, and the yield would be expected to be larger at 20 Mev, for example, than at 25 Mev. This is not in

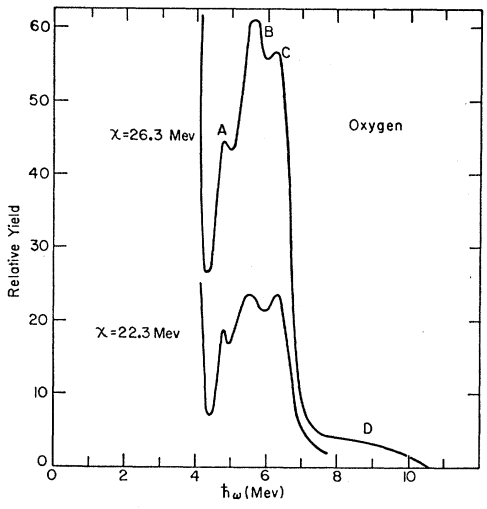

FIG. 9. The pulse-height distributions for the 4- to 10-Mev region with an O scatterer. The data were obtained at 135° and for bremsstrahlung energies of 22.3 and 26.3 Mev.

[18] Montalbetti, Katz, and Goldemberg, Phys. Rev. **91**, 659 (1953); L. Katz and A. G. W. Cameron, Can. J. Phys. **29**, 518 (1951); A. I. Berman and K. L. Brown, Phys. Rev. **96**, 83 (1954); Scott, Hanson, and Kerst, Phys. Rev. **100**, 209 (1955); V. E. Krohn Jr., and E. F. Schrader, Phys. Rev. **87**, 685 (1952).

[19] Montalbetti, Katz, and Goldemberg, Phys. Rev. **91**, 659 (1953)—the curve for Cu should be reduced by 10% (private communication).

[20] P. R. Byerly and W. E. Stephens, Phys. Rev. **83**, 54 (1951).

agreement with the measurements which indicate that the inelastic yield near 20 Mev is smaller than that near 25 Mev. Hence it is likely that the inelastic yield originates in Cu^{63} and Cu^{65}.

The data of Fig 4 were obtained with an 8 g/cm^2 scatterer. As a check, data were also obtained with a 4 g/cm^2 scatterer. The results were similar.

B. Carbon

Figure 5 shows data for carbon which were obtained from irradiations at bremsstrahlung energies of 27, 28, and 61 Mev. The points shown by crosses are for elastic scattering only, and those shown by dots are for mixed scattering. Since the first excited state of C^{12} occurs at 4.43 Mev[7] all data obtained within 4.43 Mev from the high-energy limit of a bremsstrahlung spectrum is due to elastic scattering only. It is seen that there is little, if any, inelastic scattering in the energy range 20 to 26 Mev (the 61-Mev data do not extend below 26 Mev).

The elastic scattering prediction shown by the solid curve is a modification of a previously computed curve.[21] The modification consisted of folding in the residual resolution function, $T(y)$, which is applicable to this experiment. This effects a considerable decrease in the peak height of the curve. The result is seen to be in good agreement with the measurements at 25 Mev and somewhat above them at 35 Mev. The discrepancy is not serious.

In contrast to Cu, the carbon cross section does not have the shape of a single scattering resonance and considerable photon absorption above 25 Mev is evident. This is in agreement with the measured photoneutron cross section.[22,23]

The data of Fig. 5 agree with measurements by Fuller and Hayward[21] who obtained 2.7±0.8 microbarn/sterad at 25 Mev, and about 0.9±0.5 microbarn/sterad at 35 Mev for elastic scattering.

C. Oxygen

Data for oxygen are shown in Fig. 6. They were obtained from irradiations with 22.3-, 26.4-, and 61-Mev bremsstrahlung. The crosses designate data obtained from within 6.06 Mev of the high-energy tip of the bremsstrahlung spectra and are for elastic scattering. The dots designate data which may contain inelastic scattering as well. The 61-Mev data do not extend below 24 Mev.

The scattering prediction, which is shown by the solid curve, contains the effect of the residual resolution function, $T(y)$. In contrast to the situation for Cu and C, the prediction is not in good agreement with the measurements. Furthermore, a comparison of the O and C data[24] show that the scattering cross section is considerably larger for O than for C. On the other hand, the particle photoproduction cross sections for oxygen[5,6] are smaller than those for carbon[5,21,25] by a factor of about $\frac{2}{3}$.

Detailed studies of the (γ,n) bremsstrahlung yield curve for O^{16} have shown the existence of fine structure[11] which has been taken to imply narrow resonances in the absorption cross section. This interpretation has been strengthened by studies of proton spectra from the (γ,p) reaction made with an energy resolution of about 0.2 Mev.[25] This resolution is sufficient to indicate fine structure in the cross section even though individual resonances cannot be resolved. A recent absorption experiment[26] has given a value for the average peak height of the narrow resonances near the peak of the giant resonance. The value is 106±14 mb—about five times larger than the average cross section there.

According to the discussion of Sec. II, a scattering prediction can be made from Eq. (3) if all the cross section is contained in narrow, isolated, resonances. The average absorption cross section, $\langle\bar{\sigma}_a\rangle$, which is required by Eq. (3) was obtained by adding together the measured (γ,n) and (γ,p) cross sections,[5,6] and the average peak height of the levels, $\bar{\sigma}_a{}^p$, was assumed to be five times $\langle\sigma_a\rangle$ for all energies. The resulting scattering prediction had a very strong, narrow, peak at 22.5 Mev. The residual resolution function (Fig. 2) was then folded into the predicted curve. This effected a reduction in the peak height of about a factor of two. The resulting curve had a peak height within the range shown by the light, horizontal, lines near the upper left-hand corner of Fig. 6. Thus, the observed scattering cross section is quite consistent with the conclusions of reference 26 concerning the narrow resonances.

There is a considerable uncertainty connected with the calculations just described, proceeding from the lack of accurate knowledge of the shapes of the (γ,n) and the (γ,p) cross sections for oxygen. In particular, it is not known for certain whether these two cross sections peak at the same energy, and if so, just what

TABLE I. Comparison of published values for the energy of the O^{16} giant resonance peak.

Reaction studied	Method of study	Peak energy (Mev)	Reference
$O^{16}(\gamma,n)O^{15}$	Induced activity	21.8	a
		22.7	b
$O^{16}(\gamma,p)N^{15}$	Nuclear emulsions	21.9	c
		22.3	d
		23.3	e

[a] R. Montalbetti and L. Katz, Can. J. Phys. **31**, 798 (1953).
[b] A. S. Penfold and B. M. Spicer, Phys. Rev. **100**, 1377 (1955).
[c] D. L. Livesey, Can. J. Phys. **34**, 1022 (1956).
[d] See reference 25.
[e] S. A. E. Johansson and B. Forkman, Arkiv Fysik. **12**, 359 (1957).

[21] E. G. Fuller and E. Hayward (private communication); and report to the Chicago Photonuclear Conference, 1956 (unpublished).
[22] R. Sagane, Phys. Rev. **84**, 587L (1951).
[23] Barber, George, and Reagan, Phys. Rev. **98**, 73 (1955); B. C. Cook, Phys. Rev. **106**, 300 (1957).
[24] Note: This behavior was clearly evident from the raw pulse-height spectra before any cross-section analysis was performed.
[25] Cohen, Mann, Patton, Reibel, Stephens, and Winhold, Phys. Rev. **104**, 108 (1956).
[26] A. S. Penfold and E. L. Garwin, Phys. Rev. **114**, 1324 (1959).

the peak energy is. The experimental situation is given in Table I. In making the calculations it was assumed that both cross-sections peak at 22.5 Mev, and the available cross-section measurements were adjusted accordingly.

Figure 7 shows the elastic scattering cross section for oxygen from 17 to 60 Mev (solid dots). The data were obtained from irradiations at many different betatron operating energies, and many of the points are averages of from two to four separate determinations. The cross section is seen to fall off smoothly for energies above the giant resonance, with little evidence for higher energy resonances. Between 48 and 60 Mev the cross section is apparently quite flat and slightly below the value predicted from Eq. (2) with no exchange forces. It is doubtful if any conclusions should be drawn from this behavior though, since the angular dependence of the cross section is not known at these high energies.

As in the case of carbon, the oxygen cross section does not have the shape of a single scattering resonance, and considerable photon absorption above 25 Mev is indicated. This conclusion is in agreement with another experiment.[22]

Each irradiation made to determine the elastic scattering cross section yielded, besides a few elastic points, a whole series of points for mixed scattering. The results indicated the presence of inelastic scattering for incident gamma rays above 28 Mev. The spectrum of the inelastically scattered gamma rays was observed to have a low-energy threshold of about 22 Mev. To the accuracy of the measurements, the whole inelastic yield was due to transitions to a state (or states) in O^{16} near 6 Mev. The assumption was therefore made that all the yield was due to such transitions, and Eq. (15) was applied to calculate the corresponding cross section. Owing to poor statistics, the data were averaged in bins of about 4-Mev width and only a rough idea of the cross section could be obtained. The results are shown by the triangles of Fig. 7. A line was drawn through these points in the interests of clarity, and not on the basis of any knowledge of the expected shape. Due to the liberal averaging, the cross section may in reality be considerably more peaked than the data indicate.

D. Oxygen Angular Distribution

Figure 8 shows the angular distribution which was obtained for elastically scattered gamma rays from oxygen over the energy range 19 to 25 Mev. The dashed line shows the angular distribution expected for dipole scattering. The solid line is for a mixture of noninterfering dipole and quadrupole scattering (81% dipole at 90°).

Even though the emitting states may not overlap, the quadrupole radiation should give rise to an asymmetry about 90° due to interference with the Thomson scattering. On the scale of Fig. 8 the Thomson cross section contributes a yield of 0.13 and so it is doubtful if the asymmetry would be large enough to show above the statistical uncertainty of the data.

Figure 8 confirms the assumption that the giant resonance is predominantly dipole in character.

E. Residual Gamma Rays

Figure 9 shows the results of a survey of the 4- to 9-Mev region with an oxygen scatterer. The two curves are pulse-height spectra obtained from irradiations at betatron energies of 22.3 and 26.3 Mev. The raw pulse-height spectra had points every 73 kev. The data were obtained at a detector angle of 135°.

For gamma-ray energies near 6 Mev the resolution function of the NaI detector is no longer single-peaked, but exhibits an escape peak as well as a main peak.[15] The features labelled A, B, and C in Fig. 9 are identified as follows: C is the main peak due to one or more gamma-ray lines near 6.3 Mev; part of B is the escape peak of C and part is due to one or more gamma-ray lines near 5.5 Mev; A is the escape peak of the lines at B. The ratio of the yield due to the 6.3-Mev lines to that due to the 5.5-Mev lines is about 2:1 for both curves of Fig. 9.

The area under the peaks is a sensitive function of the bremsstrahlung energy, indicating that the lines are intimately tied to processes taking place near 22 Mev. This conclusion was confirmed by two further sets of data (not shown). One, at 40-Mev bremsstrahlung energy, gave the height of the peaks as 85 on the vertical scale of Fig. 9; the other, at 19-Mev bremsstrahlung, gave the height of the peaks as about 6. It was concluded that the peaks are due to de-excitations in O^{15} and N^{15} following a (γ,p) or a (γ,n) reaction in O^{16}. The observed energies of about 6.3 and 5.5 Mev are those to be expected from such processes.[7] Part of the yield in region D, between 7 and 10 Mev, may also be due to gamma rays from O^{15} and N^{15}, but the yield is very small and individual lines are not resolved. Studies of the (γ,p) reaction[6] indicate that there is some proton emission to states in O^{15} near 9 Mev.

A previous experiment had shown the existence of residual gamma rays of about 6 Mev,[27] but the knowledge that there are two distinct groups, corresponding to transitions from states near 5.5 Mev as well as states near 6.3 Mev, is new information. The energy scale of Fig. 9 is estimated to be accurate to ± 0.2 Mev.

The angular distribution of the gamma rays forming the peaks in Fig. 9 is probably nearly isotropic. This was shown by calculating[28] the angular distributions for various combinations of multipolarities, spins, and parities which could be involved.[7] In all cases there was a strong isotropic component. Assuming isotropy, it is possible to estimate the integrated cross section which gives rise to the peaks of Fig. 9, and to compare this to the total photonuclear cross section. In

[27] N. Svantesson, Bull. Am. Phys. Soc. 1, 28 (1956).

[28] Sharp, Kennedy, Sears, and Hoyle, Atomic Energy of Canada Limited, Chalk River Report CRT-556, 1954 (unpublished).

this way it was found that 55% of the O^{16} giant resonance states decay directly to the ground states of O^{15} and N^{15}, 15% leave the residual nuclei about 5.5-Mev excited, and 30% leave the residual nuclei about 6.3-Mev excited.

Some of the yield in region *D* may be due to gamma rays which result from the interaction of photoneutrons with the NaI crystal and with the Pb shielding around it. An upper limit to this yield can be estimated by assuming a total reaction cross section for neutrons of 2.5 barns[29] and also that each reaction leads to one gamma ray of energy 4 to 10 Mev. The integrated yield which follows from the calculations is only 10% of the area under the peaks of Fig 9. The actual yield is expected to be a small fraction of this. The cause of the abrupt rise in the spectra below 4 Mev is not known, but it is not room background as this has already been subtracted.

Between 10 and 16 Mev the yield drops monotonically to a value compatible with the 16-Mev cross section shown in Fig. 7. On the vertical scale of Fig. 9 the elastic scattering yield from the "giant" resonance comes at 0.09.

VII. DISCUSSION AND CONCLUSIONS

The present results indicate that narrow, isolated, resonances play an important role in the oxygen photonuclear cross section at giant resonance energies. This conclusion is in agreement with the results of other experiments.[26,30] On the other hand, no such effect was found for carbon, a result which is also in agreement with other experiments.[26,30–32] There remains, then, the problem of interpreting the fine structure which has been observed in the $C^{12}(\gamma,n)C^{11}$ bremsstrahlung yield curve.[33]

At present, experiments indicate a decided difference in the character of the oxygen and carbon giant resonance cross sections. In particular, the states which are formed in oxygen seem to live much longer than those formed in carbon. This surprising result should be confirmed by further experiments.

The $O^{16}(\gamma,p)O^{15}$ cross section at 28 Mev has been measured[34] and is 2.3 mb. From the behavior at low energies, the total cross section can be expected to be about twice this value, say 5 mb. The peak of the observed inelastic scattering cross section for oxygen (Fig. 7) is 1.5 ± 0.25 microbarns/sterad at 135°, or 17 ± 4 microbarns total (if a dipole angular distribution is assumed). From these figures an estimate can be made of the probability that states at 30 Mev de-excite by inelastic gamma-ray emission. This probability is $\sim3.5\times10^{-3}$, probably a lower limit due to the considerable data averaging carried out in determining the inelastic cross section. On the other hand, the probability that states near *22* Mev will de-excite by *elastic* gamma-ray emission is $\sim6\times10^{-3}$ from another experiment.[26] Thus, the inelastic cross section which was observed in this experiment implies a coupling to a state (or states) near 6 Mev which is about as strong as that coupling to the ground state which gives rise to the giant resonance. This fact, along with the definite threshold and strong peak which the inelastic cross section exhibits, leads one to interpret this cross section as representing the overlap of two giant resonances—one for the ground state, and one for an excited state. Of the known states in O^{16} near 6 Mev[7] only the 0^+ state at 6.06 Mev and the 2^+ state at 6.91 Mev could be expected to couple strongly to the 1^- giant resonance states. Unfortunately, the experimental data were not sufficiently accurate to decide between these two possibilities though the evidence was in favor of the 0^+ state. If the above interpretation of the inelastic cross section is correct then a similar cross section should be observed for carbon. In that case, the 0^+ and 2^+ states are separated by 3.2 Mev[7] and an experiment would likely distinguish between them with certainty.

The concept of giant resonances for low-lying excited states which do not differ greatly in character from the ground state follows rather naturally from the giant dipole, or collective, model of the nuclear photoeffect. This is perhaps most clearly demonstrated by the treatment which has been given by Fujita [35] The peak energy of the giant resonance for the 6-Mev excited state in oxygen would be expected to be about 6 Mev higher than that for the ground-state giant resonance. This is in agreement with the present experimental observations. On the other hand, the shell model of the nuclear photoeffect would require the giant resonance for the 6-Mev state to come at nearly the same energy as that for the ground state (about 22 Mev), a conclusion which is not in agreement with this experiment.

On the basis of the alpha-particle model the 6-Mev state in O^{16} corresponds to a motion of uniform dilation[36] and so it is very similar in character to the ground state.

VII. ACKNOWLEDGMENTS

The authors would like to thank the betatron group at the National Bureau of Standards for calibrating the standard ion chamber used in this experiment. They would also like to acknowledge a useful discussion with Dr. V. L. Telegdi concerning the results of this experiment.

[29] J. M. Blatt and V. F. Weisskopf, *Theoretical Nuclear Physics* (John Wiley and Sons Inc., New York 1952), Chap. 7.
[30] A. K. M. Siddiq and R. N. H. Haslam, Can. J. Phys. **36**, 963 (1958).
[31] M. M. Wolff and W. E. Stephens, Phys. Rev. **112**, 890 (1958).
[32] L. D. Cohen and W. E. Stephens, Phys. Rev. Letters **2**, 263 (1959).
[33] Katz, Haslam, Horsley, Cameron, and Montalbetti, Phys. Rev. **95**, 464 (1954); L. Katz, Proceedings of the Washington Photonuclear Conference, 1958 (unpublished).
[34] P. Brix and E. K. Maschke, Z. Naturforsch. **12a**, 1013 (1957).
[35] J. Fujita, Progr. Theoret. Phys. (Kyoto) **16**, 112 (1956).
[36] D. M. Dennison, Phys. Rev. **57**, 454 (1940); D. R. Inglis, Revs. Modern Phys. **25**, 390 (1953).